RSC Advances

Elucidation of complexation multi-equilibrium with MgII and a multisite ligand. A combined electronic spectroscopies and DFT investigation.

Journal:	*RSC Advances*
Manuscript ID:	RA-ART-05-2014-005048
Article Type:	Paper
Date Submitted by the Author:	31-Mar-2014
Complete List of Authors:	Moncomble, Aurélien; Université Lille 1, LASIR Cornard, Jean; Université Lille 1, LASIR - Laboratoire de Spectrochimie Infrarouge et Raman

Elucidation of complexation multi-equilibrium with Mg^{II} and a multisite ligand. A combined electronic spectroscopies and DFT investigation.

Aurélien Moncomble,* Jean-Paul Cornard

LASIR – CNRS UMR8516, Université Lille 1 Sciences et Technologies, Bât C5 – 59 655 Villeneuve d'Ascq Cedex – France – aurelien.moncomble@univ-lille1.fr

Abstract

The study of the formation of complexes between quercetin, a multisite ligand, and Mg^{II} cation in solution is reported in this article. A methodology combining spectroscopic measurements and TD-DFT computations was used to study the associated monosite flavonoids and showed that the hydroxy-keto chelating power towards Mg^{II} is higher than the catechol one. In each case, the complexation occurs with one hydroxyl deprotonation. Then, by combination of absorption and emission spectra, chemometric treatments and quantum chemistry calculations, it was shown that Mg^{II} cation is involved in an equilibrium between the two hydroxyketo sites of quercetin. The coexistence in solution of two complexes C3 and C5 has been highlighted. Very different Stokes shifts were observed for these two species reflecting the structural rearrangements that occur upon complexation and excitation.

Keywords

Complex formation; Electronic spectroscopies; Magnesium; Quercetin; TD-DFT

Electronic supplementary information (ESI) available: Detailed results of least square fitting, comparison of Q, C3 and C5 geometries and cartesian coordinates for evidenced molecules.

Graphical abstract

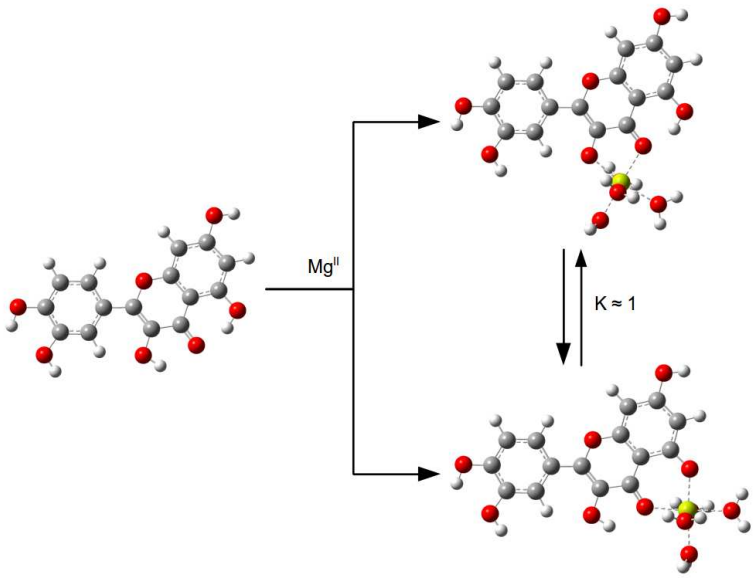

Introduction

Flavonoids form a large group of phenolic secondary metabolites of plants, widely distributed in fruits and vegetables. They have shown various biological and pharmacological activities.[1-4] Numerous epidemiological evidences that diets rich in flavonoids reduce the occurrence of chronic diseases such as cardiovascular diseases[5, 6], atherosclerosis[7], diabetes[8-10] and stroke.[11] The best known property of flavonoids is their antioxidant character towards free radicals produced either by cells metabolism or in response to external factors[12-14], that can damage biomolecules such as lipids, proteins and nucleic acids.[15] Flavonoids also form complexes with metal ions, which can affect their biological effects and notably their antioxidant activities.[16-22]

More than 9000 species have been identified in the different groups of the large family of flavonoids. Quercetin (2-(3,4-dihydroxyphenyl)-3,5,7-trihydroxy-4H-chromen-4-one), one of the most abundant natural flavonoids, is present in many plants and used as a nutritional supplement.[23] It exists in fruits and vegetables as glucosides such as rutin and quercitrin. It presents a help in the prevention of cancers, it is antioxidant, anti-diabetic and has anti-carcinogenic, anti-histamine and anti-inflammatory effects.[24] Quercetin (noted Q) presents three complexing sites in competition towards metal ions: an α-hydroxy-keto, a β-hydroxy-keto and a catechol functions. Numerous metal-Q complexes have been studied and reported in the literature[18, 25-31] but to our knowledge, the Mg^{II}-Q system has never been investigated in depth. However, Mg^{2+} is the fourth most common cation in the body and the second most common intracellular cation after K^{+}. It has a fundamental role in more than 300 enzymatic reactions involving nucleic acids.[32] Moreover, it has been shown that intracellular Mg^{2+} decreases the blocking efficiency of extracellularly applied catechol in isolated neurons, whereas catechol antagonizes the Mg^{2+}-induced shifts of the voltage-dependence of activation and inactivation.[33] Also, it was found that the complex between 3-hydroxy-flavone and Mg^{II} is formed in the excited state both from the normal and tautomer forms of the flavonol, the

latter way being more favourable.[34] Finally, the formation of a complex between Mg^{II} and 5-hydroxy-flavone was recently highlighted by various spectroscopic techniques.[35, 36] So while these three sites have been independently studied owing to their importance, their complexing powers were never compared. The main purpose of this paper is to set these sites in competition by the report of the interactions between Q and the alkaline-earth ion Mg^{II} both ubiquitous in biological systems. This system was investigated with a dual approach: electronic spectroscopies (absorption and fluorescence) and quantum chemistry calculations (density functional theory and time-dependent density functional theory-based methods). In a first step of this work, the complexation of Mg^{II} by monosite flavonoids: 3-hydroxy-flavone (3HF), 5-hydroxy-flavone (5HF) and 3',4'-dihydroxy-flavone (3'4'diHF) were investigated to class the three complexing sites according to their affinity towards the metal cation. Indeed, a complexation site of Q is found in each of these three ligands and their studies were useful to see the individual behaviour of the sites, but also (i) to test the methodology for the calculations and (ii) to determine the protonation state of the site in the presence of metal cation. In a second step, the nature of the site involved by the fixation of Mg^{II} with the multisite ligand Q was presented in details. The structure of the studied flavonoids is depicted on Figure 1, along with the atom labelling.

1. Experimental and computational methods

1.1. Reagents and chemicals

All reagents used for experiments were analytical reagent grade. Spectroscopic methanol, magnesium chloride and the four hydroxy-flavones were purchased from Sigma. The stoichiometry of the complexes was estimated by the molar ratio method[37] from the UV-visible data set. For this method, solutions containing a constant concentration (4.10^{-5} mol L^{-1}) of flavonoids in methanol

and variable concentration of Mg^{II} were used. A broad range of metal-to-ligand molar ratios (R) was used in the equilibrium studies. Ionic strength was fixed to 0.1 mol L^{-1} with NaCl.

1.2. Instrumentation

The UV-visible spectra were recorded on a Cary-l (Varian) double-beam spectrophotometer with cells of 1 cm path length, at 25°C. A flow cell was used to allow successive additions of small amounts of Mg^{II} directly in the ligand solution. The temperature of both the measurement cell and solution was controlled with a thermostatic bath. The fluorescence spectra were acquired with a Fluorolog spectrofluorimeter (Jobin-Yvon) equipped with a multichannel detector. The emission, excitation and synchronous fluorescence spectra were recorded with a band pass of 2 nm and an integration time varying from 0.1 to 0.5 s. For the synchronous spectra, different offsets were tested.

1.3. Chemometric methods

The absorption spectra collected during the course of the metal-binding experiment were analysed with the fitting program ReacLab™ Equilibria (version 1.1).[38] This software allows the determination of the number of species that contribute to the absorption spectra using a factor analysis procedure (EFA)[39-41] and of the electronic spectrum of each pure species. The ReacLab™ Equilibria software has also been used to estimate the apparent stability constants (β) of the different complexed forms. In order to obtain the best fit between the complexation model and the experimental data, several models of complexes have been envisaged for the refinement of the stability constants. The complexing power was estimated by the means of the apparent stability constant:

$$\beta = [Mg_aL_b]/([Mg]^a.[L]^b)$$

that results from the equilibrium between the free ligand L and the complex Mg_aL_b (without taking into account the protonation state of the ligand):

$$a\ Mg^{II} + b\ L = Mg_aL_b$$

The treatment of the variation temperature experiments was carried out using simple least-square methods by the formalism presented in the main text. These calculations were performed using the LibreOffice spreadsheet[42] and its extension for non-linear programming.[43]

1.4. Quantum chemistry calculations

All calculations were carried out with the Gaussian 09 set of programs.[44] Methods based upon the Density Functional Theory (DFT) and its time-dependent version (TD-DFT) were used throughout; the PBE0 global hybrid functional[45, 46] was used due to its wide domain of applicability, especially for the computation of absorption and emission properties.[47] Every atoms were represented by the 6-311+G** basis set.[48-50] Structural optimizations were realised using standard algorithms without any symmetry constraint. The nature of minima was checked by vibrational analysis. TD-DFT formalism in the adiabatic approximation was used to compute excitation energies and oscillators strengths.[51, 52] The 40 lowest excited states were taken into account to compute vertical excitation energies. The geometry optimisations of S_1 states were performed by taking into account 10 states. $NICS(0)_{iso}$[53] were computed using the GIAO method[54] at the same level of theory.

The solvent (methanol) was represented using a hemi-implicit model: the first coordination sphere around the metal cation (Mg^{II}) was completed with explicit water molecules to achieve a valence of six.[55] Then a continuum model[56] (PCM, as implemented in Gaussian with the internal parameters for methanol) was used. The solvent for emission computations was equilibrated in the first excited state. This kind of model was shown to be representative on similar systems where the electronic transitions are mainly located on ligands without influence of metal-localized orbitals; the

representation of methanol molecules by water molecules allowing to carry out more easily the computations without significant influence on the computed transition energies.[57]

2. Complexation with monosite flavonoids

2.1. Electronic spectroscopy study

Figure 2 illustrates the evolution of the electronic absorption spectra of 3HF, 5HF and 3'4'diHF with the addition of magnesium chloride, in methanol solution. In all cases, a large amount of metal salt is necessary to fully complex the ligand which tends to show that Mg^{II} complexation occurs less easily than for other metal ions such as Al^{III}, Pb^{II} or Zn^{II},[58-60] in the same experimental conditions. Typically, two major absorption maxima are observed in the UV–Vis spectrum of flavonoids. The absorption maximum observed in the range 240–285 nm is referred to as band II and the one between 300–400 nm as band I.[61] Upon complexation, the spectrum of the complexed ligand exhibits a large bathochromic shift of the band I with respect to the free ligand, for the three studied compounds. The value of these red shifts are of 66, 55 and 34 nm for 3HF, 5HF and 3'4'diHF, respectively. Band II shows less significant spectral changes. For the three monosite ligands, an isosbestic point is observed on the spectral data set, indicating the presence of an equilibrium between the free form and only one complexed form. The molar ratio method applied to the data highlights a 1:1 stoichiometry for the formed complex. Numerical treatments have been carried out to find the spectrum of the pure complexed species, especially for 3'4'diHF whose complexation is not complete even for a very high metal-to-ligand molar ratio. From chemometric method results, the stability constant of the complexes have been estimated to $\log \beta_{3HF} = 2.43 \pm 0.01$, $\log \beta_{5HF} = 2.08 \pm 0.01$ and $\log \beta_{3'4'diHF} = -0.30 \pm 0.02$ for 3HF, 5HF and 3'4'diHF, respectively. Only the value obtained for 3HF is comparable to results present in literature for Mg-flavonols (flavonoids that

have the 3-hydroxy-flavone backbone) systems, in acetonitrile, which gives values close to 2 for the logarithm of stability constants.[62] 3HF and 5HF have relatively close complexing powers, even if the stability constant of the Mg-3HF system is more than twice greater than the Mg-5HF system. In contrast, the stability constant of the Mg-3'4'diHF is lower by two orders of magnitude than that calculated for 3HF and 5HF. The catechol function presents a complexing power towards Mg^{II} clearly lower than hydroxy-keto groups and the complexing power of the three investigated sites could be classed in the following way: α-hydroxy-keto > β-hydroxy-keto >> catechol. The same order has already been obtained for Al^{III} and Zn^{II} complexation, in the same conditions (methanol, neutral medium) but where 3'4'diHF had a complexing power very close to that of 5HF.[58, 60, 63] However, it should be noted that for these last metal ions, the stability constants of the formed complexes are 10^3 times greater than those calculated for Mg^{II}.

2.2. Theoretical study

In this section, we specifically focused on the determination of the protonation state of the hydroxyl group involved in the complexation. For 3HF and 5HF, there were two possibilities: either with or without a proton on the hydroxyl. For 3'4'diHF, four possibilities were considered: fully-protonated, 3'-deprotonated, 4'-deprotonated or fully-deprotonated.

The structure of these complexes was optimized and the lowest excitations were computed. The value of the lowest transition energy for each hypothesis and the discrepancy with the experimental value are reported in Table 1.

The comparison between the computed and the experimental wavelengths reported in this table allows in the two first cases an unambiguous determination of the complexes structures: the complexation of the Mg^{II} cation occurs with the α-hydroxy-keto and the β-hydroxy-keto moiety of 3HF and 5HF, respectively. In both cases, the hydroxyl group involved is deprotonated. The whole

spectra are depicted on Figures 3 and 4 and show a good agreement between the computed data and the general features of the experimental spectra.

In the case of 3'4'diHF, the wavelengths reported in Table 1 show that the fixation of the magnesium(II) cation to the catechol group leads to a single deprotonation instead of the double deprotonation that could have been expected. The structure could be determined by considering the whole spectrum (Fig. 5): the general features are better reproduced when the deprotonation occurs on the 4'-hydroxyl group. This is consistent with the fact that a charge on the 4'-oxygen is possibly more delocalised than on the 3'-oxygen (that is justified by resonance forms).

In every cases, the lowest energy excitation involves mainly the HOMO → LUMO transition (more than 98%). These orbitals are depicted on Figure 6. Some common features should be noticed. First, the transitions are nearly exclusively localised on the ligand with only a very low contribution of the cation. Second, the main character of the lowest transition is a charge transfer from the hydroxyl groups to an orbital containing a strong C=O π^* component. One should notice that the B ring is not involved in the HOMO of 5HF. This is linked to the non-planarity of this molecule: whereas the dihedral angle between the B ring and the chromone moiety is 0.2° and 2.7° for the 3HF and the 3'4'diHF complexes, respectively; this angle yields 18.5° in the 5HF one. This planarity effect has already been studied in our group.[64]

The good agreement between the experimental and theoretical spectral properties validates the approach we proposed and allows to go further in the study of a multisite ligand: quercetin.

3. Complexation with quercetin

3.1. UV-visible spectroscopy study

The UV-visible absorption spectrum of free Q in methanol is mainly characterized by an important absorption band at 372 nm (band I) and a second one located at 255 nm (band II) with a shoulder at 269 nm. Significant spectral changes are observed with successive additions of small amount of Mg^{II} (Fig. 7). The band I of the complexed form of Q shifts to 416 nm (red shift of 44 nm) and a new and less intense band appears at 339 nm, whereas the bathochromic shift of band II is less pronounced (267 nm). The molar ratio method applied at the absorption maximum of Q to the data highlights a 1:1 stoichiometry for the formed complex. Numerical treatments have been carried out to find the spectrum of the pure complexed species.

3.2. Quantum chemistry study

As for the study of monosite complexes, the structure of some hypothetical complexes was optimized and the lowest excitations were computed. The nature of these complexes, the value of the lowest transition energy for each hypothesis and the discrepancy with the experimental value are reported in Table 2.

These values exclude the formation of a complex involving the catechol group. Indeed, whatever the protonation state of the hypothetical complex, the computed wavelength is quite far from the experimental value. This result is consistent with the computed complexation constants for the monosite flavonoids (see section 2 this article) that have shown that Mg^{II} possesses a very moderate affinity for catechol.

Two structural hypotheses seem to suit the experimental value: the complexation with the deprotonated α-hydroxy-keto and the complexation with the deprotonated β-hydroxy-keto (bold in Table 2, these complexes will be denoted as C3 and C5 in the following, respectively, see Fig. 8). The proximity of the computed wavelengths did not allow a definite attribution of the structure of the complex formed during the experiment. To discriminate between the two still hypotheses, the

new band appeared at 339 nm (denoted as band I') was then used. The two lowest absorption energies are reported in Table 3. In both cases, a very good agreement between the two computed wavelengths and the experimental values is obtained. Moreover, the experimental complex spectrum with the computed transitions for the two hypotheses are represented in Figure 8: the two computed spectra are consistent when considering only the wavelengths, but the ratio between the intensities of the two low-energy bands is badly reproduced by each spectrum. The oscillator strength calculated for the band observed at 339 nm seems underestimated in the case of C3 and overestimated in the case of C5. Once again, we were not able do conclude from this data.

From the structural point of view (see Supporting Information for a Table with the most significant parameters), the two complexes present several similarities: the two C—O bond involved in the complexation are coplanar and the magnesium atom is in the same plane. Moreover, the B ring is nearly coplanar with the chromone moiety: the dihedral angle is lower than 1° in both cases, to be compared to the value in free Q (4.4°); this planarity effect (to be compared with the important angle present in the complex with 5HF) is due to the presence of an hydroxyl group in position 3. About the bond lengths, in both cases, the C4—O4 bond is longer after complexation whereas the other C—O bond involved in the complexation is shortened. This should be related to the strongly ionic character of the O—Metal bond that was shown in the case of aluminium on a β-hydroxy-keto site in a previous work.[57] Above these expected modifications, the only other important (more than 1 pm) alteration observed while the C3 complex is formed is the lengthening of the C2—C3 bond. On the contrary, several bonds of the ligand are altered by the formation of the C5 complex: it is the case of C10—C9, C9—C8, C8—C7 and C7—C6, all located on the A ring whose aromatic character is then affected by the complexation. The effect on the aromaticity of C5 is confirmed by two evaluations of the aromaticity of the A ring: (i) the standard deviation among the CC bonds on the A ring is lower in C5 than in C3 (2.4 and 1.5 pm, respectively); (ii) the computation of $NICS(0)_{iso}$ for the A ring leads to a value of -10.3 ppm in Q to be compared to -10.1 ppm and -

8.2 ppm in C3 and C5, respectively. The value of the $NICS(0)_{iso}$ for the C ring is quite high (-3.2 ppm) that confirms the very low aromatic character of this ring.

As presented for the monosite ligands, the complexing power towards Mg^{II} of the two corresponding sites are close. This lead us to focus on another possibility: the coexistence in significant amount of both C3 and C5 complexes in the reaction mixture; so, a combination of both spectra would lead to a good reproduction of the relative intensities of both low-energy bands. In this case, the concentrations of the two complexes would be proportional that forbids the separation of their respective contribution to the total spectrum in the absence of the variation of another parameter that varies the equilibrium.

3.3. Variable temperature study

To challenge this hypothesis, we studied the evolution of the absorption spectra with temperature (in the range 10-50°C). A large excess of Mg^{2+} (R = 700) was added to a solution of quercetin ($c = 4.10^{-5}$ mol L^{-1}) to ensure a nearly total complexation of the ligand. The spectra were recorded by step of 5°C and reported on Figure 9.

When increasing the temperature, a bathochromic effect is observed on the band I while a hypochromic one is observed on the band I'. These two phenomenons did not correspond to the displacement of the simple equilibrium between the free ligand and a complex that would imply a variation in intensity of the band I. Considering the computed wavelengths and the oscillators strengths (Fig. 8), the spectral changes could arise from the conversion of C5 to C3 by an endothermic reaction, this equilibrium being displaced by the temperature variation. Indeed, C5 has a higher calculated oscillator strength around 340 nm and C3 presents a calculated absorption higher in wavelength than C5 around 420 nm.

To go further in this analysis, we proceeded to a quantitative treatment of the data obtained with the temperature variation. In the 360-450 nm spectral range, only three components contribute significantly to the absorption: the two complexes contribute to the band I while only C5 contributes to the band I'. If the contribution of a complex to an absorption band is represented by a gaussian function, one can write (considering that the molar extinction coefficient does not vary with temperature):

$$\varepsilon_3(\lambda) = a_3\, G_3(\lambda) \qquad (1)$$

$$\varepsilon_5(\lambda) = a_5\, [\, G_{5,1}(\lambda) + x_5\, G_{5,2}(\lambda)\,] \qquad (2)$$

with ε_3 and ε_5 being the molar extinction coefficient of C3 and C5, respectively, and G_i denoting normalized gaussian functions (whose centres μ_i and widths σ_i are not precised in order to have lighter expressions), a_i denoting coefficients for the linear combination and x_5 being the ratio between the two lowest bands contained in the spectrum of C5.

By combination of (1) and (2) with the Beer-Lambert law for the resulting absorption of a mixture containing the two complexes at a given temperature, one obtains (with l the optical path length and c_i the concentrations):

$$A(\lambda,T) = l\, [\, c_3(T)\, \varepsilon_3(\lambda) + c_5(T)\, \varepsilon_5(\lambda)\,]$$

that can be rewritten as:

$$A(\lambda,T) = \eta_3(T)\, G_3(\lambda) + \eta_5(T)\, [\, G_{5,1}(\lambda) + x_5\, G_{5,2}(\lambda)\,] \qquad (3)$$

with $\eta_i(T) = l\, c_i(T)\, a_i$

A least-square method was applied to the difference between the experimental spectra and the one computed with expression (3) (by step of 1 nm on the 360-450 nm range) varying parameters for the three gaussian functions and the η_i coefficients. Centres and widths of the gaussian functions are reported in Table 4, the other parameters (η_i and x_5) are given in Supporting Information.

The wavelengths obtained from this analysis (μ_i) are in very good agreement with those computed by TD-DFT, the low discrepancy observed can be attributed to the important approximations that

have been carried out, especially the fact to describe the absorption by only three gaussian functions in the studied range.

Moreover, from the definition of η_i, the concentration profile of the two complexes can be obtained as represented on Figure 10. The total concentration of ligand is nowhere imposed in the model so the constance of the sum of both concentrations is a quality criterion that appears to be achieved in this case. The concentrations appear to be very close, explaining the general features of the experimental spectrum given Figure 8, and notably the intensity ratio of band I and I'. Moreover, the variation of the concentrations on this temperature range are low that explains the minor observed spectral changes.

The concentrations of both species are linked by the means of the constant reaction.

C5 = C3 K

The concentration profile was fitted (using a least-square method) by this model, allowing the determination of the thermodynamic quantities of the transformation:

$\Delta_r H° = 2.0$ kcal mol^{-1}

$\Delta_r S° = 6.4$ cal mol^{-1} K^{-1}

The transformation is endothermic, consistently with the previous examination of the spectral evolution with temperature.

Knowing the concentrations for each temperature, we were able to separate from the spectra given on Figure 9 the main contributions of the two complexes: another least-square method was applied to fit the data using as parameters the molar absorption coefficients of both complexes at a given wavelength (neglecting their variation with temperature). These values were computed with a step of 5 nm with a constraint of positivity of the absorption. The obtained spectra are depicted on Figure 11. Due to the several levels of approximation until this part, only the general shape should

be examined and not the quantitative features. The shape of both spectra is consistent with the TD-DFT computed ones.

3.4. Fluorescence spectroscopy studies

If optical absorption of the two complexes is very close, one can imagine that their fluorescence emission is more distinct, which would strengthen our hypothesis of the coexistence of two species in solution. For this reason, emission, synchronous and excitation fluorescence measurements were carried out on a methanol solution of complex obtained with a very large excess of Mg^{II} (molar ratio of 700). Figure 12a shows the evolution of the fluorescence emission spectrum of the complex with the excitation wavelength. The observed changes in fluorescence intensity can be mainly explained by the absorbance variations with the excitation wavelength. In opposition, the fluorescence shift arises, without any doubt, from the presence of two fluorescent species in solution. The maximum emission wavelength varies between two limits, 485 and 514 nm; these last values must be located between the maximum emission wavelengths of the two complexes.

The intensity maximum of emission is observed for an excitation near 430 nm, and not at 418 nm that corresponds to the absorption maximum in the UV-visible spectrum. Considering that the value associated with 418 nm is a linear combination of absorptions of the two complexes, this finding means that absorbing species at higher wavelengths, C3, presents a higher fluorescence quantum yield than C5. It also means that the emission observed at 485 nm has for main origin the complex C3 while that observed at 514 nm corresponds rather to the fluorescence of the complexed species C5. Indeed, an excitation at 350 nm, in a spectral range where the absorption of C5 complex has a comfortable majority, leads to the recording of an emission band centred on 514 nm. The same band is observed when an excitation in the foot of the absorption band (near 480 nm) is used. This finding suggests that if the absorption band of C5 complex has a λ_{max} lower than the one of C3

complex, the first one has a larger bandwidth; this confirms previous calculations that led to a $G_{5,1}$ width larger than G3 width.

The structures were optimized in the first excited state by TD-DFT and have lead to fluorescence emission wavelengths. The results of these calculations give an emission wavelength of 502 and 511 nm for C3 and C5 complex, respectively. These values are in agreement with experimental data and indicate notably that if C5 has an absorption wavelength lower than C3, it presents a higher emission wavelength than C3. A great difference is then observed in the Stokes shifts of the two complexed forms. This important disparity in the Stokes shifts is illustrated with the synchronous fluorescence spectra reported on Figure 12b. An emission maximum is observed at 486 nm, characteristic of C3, with an offset of 50 nm whereas an offset of 100 nm leads to band located at 508 nm corresponding to C5. Moreover, the values of the calculated oscillator strengths (0.799 and 0.292 for C3 and C5, respectively) confirm that C3 is a more fluorescing species than C5.

Finally, to obtain directly a spectral absorption profile, fluorescence excitation spectra have been recorded by observing the signal at different wavelengths (Fig. 12c). Although the absorption bands of the two complexed species are very close and the fluorescence of the C3 complex signal masks widely the C5 signal, it is still possible to show that the band observed at 339 nm is essentially due to the absorption of C5 complex. Indeed, the spectrum recorded at an emission wavelength of 487 nm (complex C3) shows a very important intensity ratio between the bands observed at 438 and 339 nm, while intensities of these two bands are of the same order of magnitude when the spectrum is recorded at an emission wavelength of 600 nm (complex C5). These intensity ratios are in very good agreement with those of oscillator strengths calculated by TD-DFT.

To shed some light on the large difference between the two Stokes shifts, we proceeded to a detailed structural study of the changes implied by the $S_0 \rightarrow S_1$ transition (see supporting information for detailed data). Five bonds are strongly affected (variation above 2.5 pm) by the excitation of C3: the

two O—Mg (one shorter, one longer), the C4—O4 (longer), the C2—C1 (shorter) and the C2—C3 (longer) bonds. This is consistent with the nature of the transition that is mainly a transfer from the hydroxyl groups (including 3' and 4' ones) to an orbital having a strong C=O π^* character (as in the monosite ligands). Interestingly, much more bonds are affected during the excitation of C5: in addition of the five bonds corresponding to those of C3, six other bonds show an important change, dispersed on the whole chromone part. Moreover, among the three of them that are localised on the A ring (C8—C9, C9—C10 and C6—C7), the two last are also strongly modified by the formation of the complex C5, but in the opposite sense. This allows to propose a synthetic explanation for the very important Stokes shift obtained for C5 by comparison with C3: the formation of C5 implies a distortion of the A ring that leads to an alteration of its aromaticity character; the excitation of this complex allows a release of this constraint by increasing the O4 charge, leading to a lengthening of the Mg—O5 distance.

Conclusion

This study allows by the combination of several spectroscopic measurements, chemometric treatment of the data and quantum chemistry computations to show the coexistence of two complexes in the presence of magnesium(II) and quercetin in solution. To our knowledge, it is the first time that an equilibrium between two 1:1 complexes is evidenced in solution involving two different sites on this kind of ligands. The general formula is in each case $[Mg(C_{15}H_9O_7)(solvent)_5]^+$ and this study shows that the hydroxy-keto (either α or β) functions have chelating ability towards the magnesium(II) higher than catechol group and liberate a proton in these conditions. These results are consistent with those obtained for monosites flavonoids. The very good agreement obtained between wavelengths obtained with the wide variety of used methods (Table 5) allows to be very confident in the overview on the complex medium presented in this article. TD-DFT

computations reproduce and explain the large difference between the Stokes shift of the two complexes present in solution. Moreover, this study exemplifies the necessity to focus several experimental and theoretical methods to acquire a good comprehension of this kind of systems.

Acknowledgements

The authors are very grateful to Jérémy Gaillard for spectra measurements and to Axel Dhondt for preliminary computations on these systems. Furthermore, this work was granted access to the HPC resources of CINES and IDRIS under the allocation 2014-086933 made by GENCI (Grand Equipement National de Calcul Intensif). We also thank the CRI (Centre de Ressources Informatiques) of the Université Lille 1 for providing computing time for part of the theoretical calculations.

References

1. M. R. Fesen, Y. Pommier, F. Leteurtre, S. Hiroguchi, J. Yung and K. W. Kohn, *Biochem. Pharmacol.*, 1994, **48**, 595-608.
2. B. Havsteen, *Biochem. Pharmacol.*, 1983, **32**, 1141-1148.
3. A. Constantinou, R. Mehta, C. Runyan, K. Rao, A. Vaughan and R. Moon, *J. Nat. Prod.*, 2004, **58**, 217-225.
4. A. Daniel Boese and E. Codorniu-Hernandez, *Phys. Chem. Chem. Phys.*, 2012, **14**, 15682-15692.
5. P. A. Tsuji, K. K. Stephenson, K. L. Wade, H. Liu and J. W. Fahey, *Nutr. Cancer*, 2013, **65**, 1014-1025.
6. E. Napoleone, A. Cutrone, F. Zurlo, A. Di Castelnuovo, M. D'Imperio, L. Giordano, A. De Curtis, L. Iacoviello, D. Rotilio, C. Cerletti, G. de Gaetano, M. B. Donati and R. Lorenzet, *Thromb. Res.*, 2013, **132**, 288-292.
7. J. Reed, *Crit. Rev. Food Sci. Nutr.*, 2002, **42**, 301-316.
8. H. W. Si, Z. Fu, P. V. A. Babu, W. Zhen, T. LeRoith, M. P. Meaney, K. A. Voelker, Z. Q. Jia, R. W. Grange and D. M. Liu, *J. Nutr.*, 2011, **141**, 1095-1100.
9. R. Zamora-Ros, N. G. Forouhi, S. J. Sharp, C. A. Gonzalez, B. Buijsse, M. Guevara, Y. T. van der Schouw, P. Amiano, H. Boeing, L. Bredsdorff, F. Clavel-Chapelon, G. Fagherazzi, E. J. Feskens, P. W. Franks, S. Grioni, V. Katzke, T. J. Key, K. T. Khaw, T. Kuhn, G. Masala, A. Mattiello, E. Molina-Montes, P. M. Nilsson, K. Overvad, F. Perquier, J. R. Quiros, I. Romieu, C. Sacerdote, A. Scalbert, M. Schulze, N. Slimani, A. M. W. Spijkerman, A. Tjonneland, M. J. Tormo, R. Tumino, D. L. van der A, C. Langenberg, E. Riboli and N. J. Wareham, *Diabetes Care*, 2013, **36**, 3961-3970.
10. D. Margina, D. Gradinaru, G. Manda, I. Neagoe and M. Ilie, *Food Chem. Toxicol.*, 2013, **61**, 86-93.

11. L. Arab, F. Khan and H. Lam, *Am. J. Clin. Nutr.*, 2013, **98**, 1651S-1659S.

12. M. Leopoldini, N. Russo and M. Toscano, *Food Chem.*, 2011, **125**, 288-306.

13. Z. Y. Chen, P. T. Chan, K. Y. Ho, K. P. Fung and J. Wang, *Chem. Phys. Lipids*, 1996, **79**, 157-163.

14. S. V. Jovanovic, S. Steenken, M. Tosic, B. Marjanovic and M. G. Simic, *J. Am. Chem.Soc.*, 1994, **116**, 4846-4851.

15. P. A. Grace, *Br. J. Surg.*, 1994, **81**, 637-647.

16. A. M. Bondzic, T. D. Lazarevic-Pasti, B. P. Bondzic, M. B. Colovic, M. B. Jadranin and V. M. Vasic, *New J. Chem.*, 2013, **37**, 901-908.

17. I. Esparza, Í. Salinas, C. Santamaría, J. M. García-Mina and J. M. Fernández, *Anal. Chim. Acta*, 2005, **543**, 267-274.

18. J. M. Dimitrić Marković, Z. S. Marković, T. P. Brdarić, V. M. Pavelkić and M. B. Jadranin, *Food Chem.*, 2011, **129**, 1567-1577.

19. M. T. Fernandez, M. L. Mira, M. H. Florêncio and K. R. Jennings, *J. Inorg. Biochem.*, 2002, **92**, 105-111.

20. R. Ravichandran, M. Rajendran and D. Devapiriam, *Food Chem.*, 2014, **146**, 472-478.

21. M. L. Guo, C. Perez, Y. B. Wei, E. Rapoza, G. Su, F. Bou-Abdallah and N. D. Chasteen, *Dalton Trans.*, 2007, 4951-4961.

22. J. Dimitrić Marković, D. Amić, B. Lučić and Z. Marković, *Monatsh. Chem.*, 2014, 1-7.

23. M. J. Ko, C. I. Cheigh, S. W. Cho and M. S. Chung, *J. Food Eng.*, 2011, **102**, 327-333.

24. M. Harwood, B. Danielewska-Nikiel, J. F. Borzelleca, G. W. Flamm, G. M. Williams and T. C. Lines, *Food Chem. Toxicol.* , 2007, **45**, 2179-2205.

25. J. P. Cornard, L. Dangleterre and C. Lapouge, *J. Phys. Chem. A*, 2005, **109**, 10044-10051.

26. J. P. Cornard and J. C. Merlin, *Journal of Inorganic Biochemistry*, 2002, **92**, 19-27.

27. J. P. Cornard and J. C. Merlin, *Polyhedron*, 2002, **21**, 2801-2810.

28. A. Gülsen, B. Turan, D. P. Makris and P. Kefalas, *Eur. Food Res. Technol.*, 2007, **225**, 435–441.

29. T. Jun, W. Bochu and Z. Liancai, *Colloids Surf. B*, 2007, **55**, 149-152.

30. G. Le Nest, O. Caille, M. Woudstra, S. Roche, B. Burlat, V. Belle, B. Guigliarelli and D. Lexa, *Inorg. Chim. Acta*, 2004, **357**, 2027-2037.

31. M. Leopoldini, N. Russo, S. Chiodo and M. Toscano, *J. Agric. Food Chem.*, 2006, **54**, 6343-6351.

32. W. J. Fawcett, E. J. Haxby and D. A. Male, *Br. J. Anaesth.*, 1999, **83**, 302-320.

33. L. Erdélyi, V. I. Ilyin, N. A. Lozovaya and C. A. Vulfius, *Neurosci. Lett.*, 1990, **117**, 99-104.

34. A. D. Roshal, A. V. Grigorovich, A. O. Doroshenko, V. G. Pivovarenko and A. P. Demchenko, *J. Photochem. Photobiol. A* 1999, **127**, 89-100.

35. V. Uivarosi, M. Badea, R. Olar, C. Drăghici and S. F. Bărbuceanu, *Molecules*, 2013, **18**, 7631-7645.

36. V. Uivarosi, E. M. Pahontu and A. Munteanu, *Rev. Chim.*, 2014, **65**, 33-38.

37. A. E. Martel and R. D. Hancock, *Metal complexes in aqueous solutions*, Plenum, New York, 1996.

38. *ReactLab Equilibria*, Jplus Consulting, Kawara, Australia.

39. H. Gampp, M. Maeder, C. J. Meyer and A. Zuberbühler, *Talanta*, 1986, **33**, 943.

40. H. Gampp, M. Maeder and A. D. Zuberbühler, *Trends Anal. Chem.*, 1988, **7**, 111-113.

41. M. Maeder and A. D. Zuberbühler, *Anal. Chem.*, 1990, **62**, 2220.

42. *LibreOffice Calc*, 4.1, The Document Foundation, Berlin, 2013.

43. *Solver for non-linear programming*, 0.9, Sun Microsystems, Inc., Santa Clara, 2009.

44. M. J. Frisch, G. W. Trucks, H. B. Schlegel, G. E. Scuseria, M. A. Robb, J. R. Cheeseman, G. Scalmani, V. Barone, B. Mennucci, G. A. Petersson, H. Nakatsuji, M. Caricato, X. Li, H. P. Hratchian, A. F. Izmaylov, J. Bloino, G. Zheng, J. L. Sonnenberg, M. Hada, M. Ehara, K.

Toyota, R. Fukuda, J. Hasegawa, M. Ishida, T. Nakajima, Y. Honda, O. Kitao, H. Nakai, T. Vreven, J. A. J. Montgomery, J. E. Peralta, F. Ogliaro, M. Bearpark, J. J. Heyd, E. Brothers, K. N. Kudin, V. N. Staroverov, R. Kobayashi, J. Normand, K. Raghavachari, A. Rendell, J. C. Burant, S. S. Iyengar, J. Tomasi, M. Cossi, N. Rega, N. J. Millam, M. Klene, J. E. Knox, J. B. Cross, V. Bakken, C. Adamo, J. Jaramillo, R. Gomperts, R. E. Stratmann, O. Yazyev, A. J. Austin, R. Cammi, C. Pomelli, J. W. Ochterski, R. L. Martin, K. Morokuma, V. G. Zakrzewski, G. A. Voth, P. Salvador, J. J. Dannenberg, S. Dapprich, A. D. Daniels, Ö. Farkas, J. B. Foresman, J. V. Ortiz, J. Cioslowski and D. J. Fox, *Gaussian 09, Revision D.01*, Gaussian, Inc., Wallingford CT, 2009.

45. J. P. Perdew, K. Burke and M. Ernzerhof, *Phys. Rev. Lett.*, 1997, **78**, 1396-1396.

46. C. Adamo and V. Barone, *J. Chem. Phys.*, 1999, **110**, 6158-6170.

47. D. Jacquemin, E. A. Perpète, G. E. Scuseria, I. Ciofini and C. Adamo, *J. Chem. Theory Comput.*, 2007, **4**, 123-135.

48. R. Krishnan, J. S. Binkley, R. Seeger and J. A. Pople, *J. Chem. Phys.*, 1980, **72**, 650-654.

49. A. D. McLean and G. S. Chandler, *J. Chem. Phys.*, 1980, **72**, 5639-5648.

50. T. Clark, J. Chandrasekhar, G. W. Spitznagel and P. V. R. Schleyer, *J. Comput. Chem.*, 1983, **4**, 294-301.

51. R. Bauernschmitt and R. Ahlrichs, *Chem. Phys. Lett.*, 1996, **256**, 454-464.

52. R. E. Stratmann, G. E. Scuseria and M. J. Frisch, *J. Chem. Phys.*, 1998, **109**, 8218-8224.

53. A. Ebrahimi, P. Karimi, F. B. Akher, R. Behazin and N. Mostafavi, *Mol. Phys.*, 2013, **112**, 1047-1056.

54. R. Ditchfield, *Mol. Phys.*, 1974, **27**, 789-807.

55. D. T. Richens, *The Chemistry of Aqua Ions*, John Wiley & Sons Inc 1997.

56. J. Tomasi, B. Mennucci and R. Cammi, *Chem. Rev.*, 2005, **105**, 2999-3094.

57. S. Say-Liang-Fat, J.-P. Cornard and A. Moncomble, *Polyhedron*, 2012, **48**, 237-244.

58. J. P. Cornard and J. C. Merlin, *J. Mol. Struct.*, 2003, **651-653**, 381-387.

59. C. Lapouge and J. P. Cornard, *J. Phys. Chem. A*, 2005, **109**, 6752-6761.

60. J. P. Cornard, L. Dangleterre and C. Lapouge, *Chem. Phys. Lett.*, 2006, **419**, 304-308.

61. T. J. Mabry, K. R. Markham and M. B. Thomas, *The Systematic Identification of Flavonoids*, Springer-Verlag: New York, NY, USA, 1970.

62. A. D. Roshal, A. V. Grigorovich, A. O. Doroshenko, V. G. Pivovarenko and A. P. Demchenko, *J. Phys. Chem. A*, 1998, **102**, 5907-5914.

63. C. Lapouge, L. Dangleterre and J. P. Cornard, *J. Phys. Chem. A*, 2006, **110**, 12494-12500.

64. G. Lewin, A. Maciuk, A. Moncomble and J.-P. Cornard, *J. Nat. Prod.*, 2012, **76**, 8-12.

Table 1: Lowest energy transition wavelength and oscillator strength for the different protonation states of the complexes formed between the three studied monosite flavonoids and Mg^{II} cation.

Flavone	Protonation state	Absorption lowest energy (in nm (eV))	Discrepancy with experiment (in nm (eV))	Oscillator strength
3HF	Fully-protonated	322 (3.85)	89 (0.83)	0.401
	3OH-deprotonated	**407 (3.05)**	**4 (0.03)**	**0.465**
	Experiment	*411 (3.02)*		
5HF	Fully-protonated	321 (3.86)	71 (0.70)	0.339
	5OH-deprotonated	**411 (3.02)**	**19 (0.14)**	**0.084**
	Experiment	*392 (3.16)*		
3'4'diHF	Fully-protonated	323 (3.83)	55 (0.60)	0.004
	3'OH-deprotonated	372 (3.33)	6 (0.05)	0.151
	4'OH-deprotonated	**363 (3.42)**	**15 (0.14)**	**0.767**
	Fully-deprotonated	457 (2.71)	79 (0.57)	0.382
	Experiment	*378 (3.28)*		

Table 2: Lowest energy transition wavelength and oscillator strength for the different protonation states of the hypothetical complexes formed between the quercetin and Mg^{II} cation.

Site	Protonation state	Absorption lowest energy (in nm (eV))	Discrepancy with experiment (in nm (eV))	Oscillator strength
α-hydroxyketo	Fully-protonated	375 (3.31)	41 (0.33)	0.496
	3OH-deprotonated	**420 (2.96)**	**4 (0.02)**	**0.580**
β-hydroxyketo	Fully-protonated	394 (3.15)	22 (0.17)	0.703
	5OH-deprotonated	**411 (3.01)**	**5 (0.03)**	**0.341**
catechol	Fully-protonated	366 (3.39)	50 (0.41)	0.417
	3'OH-deprotonated	397 (3.13)	19 (0.15)	0.248
	4'OH-deprotonated	393 (3.16)	23 (0.18)	0.843
	Fully-deprotonated	483 (2.57)	67 (0.41)	0.482
Experiment (1:1 complex)		*416 (2.98)*		

Table 3: Two lowest energy transition wavelengths, oscillator strength and nature of the transition (H stands for HOMO and L for LUMO) for the deprotonated complexes formed between the quercetin and Mg^{II} cation. Only transitions with a contribution over 5% are reported.

Complex	Absorption lowest energy (in nm (eV))	Discrepancy with experiment (in nm (eV))	Oscillator strength	Nature of the transition
C3	420 (2.96)	4 (0.02)	0.580	H → L (99%)
	328 (3.78)	12 (0.16)	0.045	H - 1 → L (94%)
C5	411 (3.01)	5 (0.03)	0.341	H → L (95%)
	342 (3.62)	3 (0.04)	0.372	H - 1 → L (95%)
Experiment (1:1 complex)	*416 (2.98)* *339 (3.66)*			

Table 4: Centres and widths obtained for each gaussian function from the analysis of the spectra obtained by variation of temperature (centres given in nm (eV), widths in cm^{-1} (eV)).

	G_3	$G_{5,1}$	$G_{5,2}$
μ_i	429 (2.89)	399 (3.11)	331 (3.75)
σ_i	1104 (0.14)	1357 (0.17)	1920 (0.24)

Table 5: Comparison of the transition wavelengths (absorption and emission) obtained by different (experimental and theoretical) methods for the complexes C3 and C5 (values given in nm (eV)).

		C3	C5
Absorption	Direct measurement	416 (2.98); 339 (3.66)*	
	TD-DFT	420 (2.95)	411 (3.02); 342 (3.63)
	Temperature variation	429 (2.89)	399 (3.11); 331 (3.75)
	Fluorescence excitation	438 (2.83)	–**; 338 (3.67)
Emission	Direct measurement	485 (2.56)	514 (2.41)
	TD-DFT	502 (2.47)	511 (2.43)
	Synchronous fluorescence	486 (2.55)	508 (2.44)

* impossible to differentiate the two complexes

** no value was obtained from this method for the band I of C5

Figures captions

Figure 1: Atomic numbering and substitution pattern of the studied flavonoids with the notation used in the text.

Figure 2: UV-vis spectra in methanol, in the absence and in the presence of Mg^{II} for (a) 3HF for molar ratio varying from 0 to 450, (b) 5HF for molar ratio varying from 0 to 950 and (c) 3'4'diHF for molar ratio varying from 0 to 9000.

Figure 3: Computed transitions (blue vertical lines) and experimental spectrum (black) for 3HF-Mg^{II} complex. (a) protonated structure; (b) deprotonated structure.

Figure 4: Computed transitions (blue vertical lines) and experimental spectrum (black) for 5HF-Mg^{II} complex. (a) protonated structure; (b) deprotonated structure.

Figure 5: Computed transitions (blue vertical lines) and experimental spectrum (black) for 3'4'diHF-Mg^{II} complex. (a) protonated structure; (b) fully-deprotonated structure; (c) 3'-deprotonated structure; (d) 4'-deprotonated structure.

Figure 6: Representation of the HOMO and the LUMO of the three formed monosite complexes.

Figure 7: UV-vis spectra in methanol, in the absence and in the presence of Mg^{II}, for Q for molar ratio varying from 0 to 700.

Figure 8: Computed transitions (blue vertical lines) and experimental spectrum (black) for Q-Mg^{II}

complex. (a) fixation on the 3-hydroxyketo; (b) fixation on the 5-hydroxyketo; (c) fixation on the catechol.

Figure 9: Evolution of the spectrum of the mixture Q-Mg^{II} with temperature. The arrows indicate the variations from 10°C to 50°C by 5°C step.

Figure 10: Concentration profile of the two complexes as a function of the temperature.

Figure 11: Pure absorption spectra of C3 and C5 extracted from the temperature variation experiment.

Figure 12: Fluorescence spectra for Q-Mg^{II} complex. (a) Emission spectra obtained for different excitation wavelengths (noted in nm on each spectrum). The intensity of three spectra has been multiplied by a factor 5; (b) Synchronous spectra recorded with offsets of 50 and 100 nm; (c) Excitation spectra recorded at different wavelengths (noted in nm on each spectrum). The intensity of the spectrum recorded in the band foot has been multiplied by a factor 15. For a purpose of comparison, absorption spectrum is added on the figure.

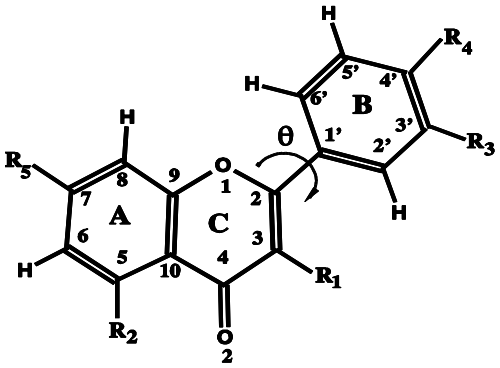

Compounds	Notation	R1	R2	R3	R4	R5
3-hydroxyflavone	3HF	OH	H	H	H	H
5-hydroxyflavone	5HF	H	OH	H	H	H
3',4'-dihydroxyflavone	3'4'diHF	H	H	OH	OH	H
quercetin	Q	OH	OH	OH	OH	OH

Fig. 1

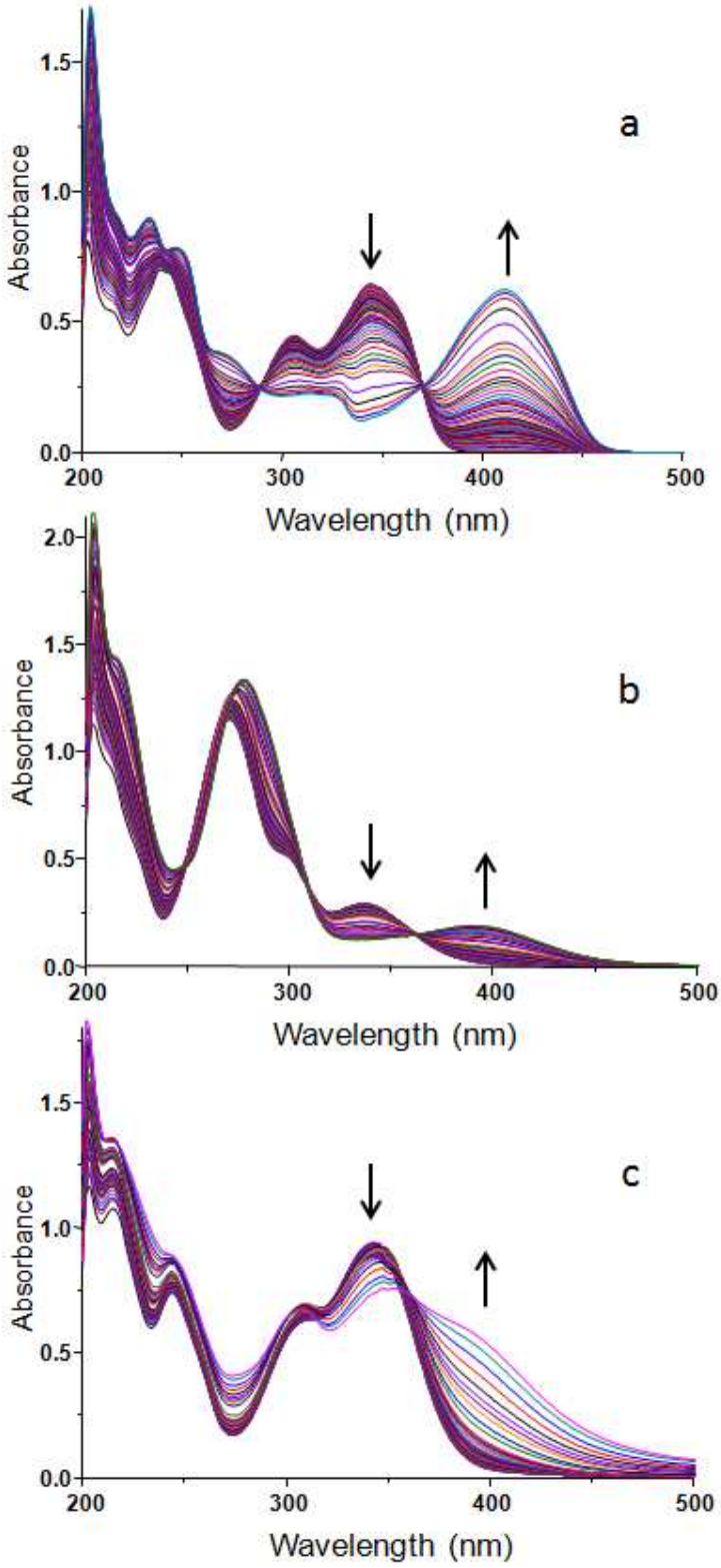
a
Absorbance
Wavelength (nm)
b
Absorbance
Wavelength (nm)
c
Absorbance
Wavelength (nm)

Fig. 2

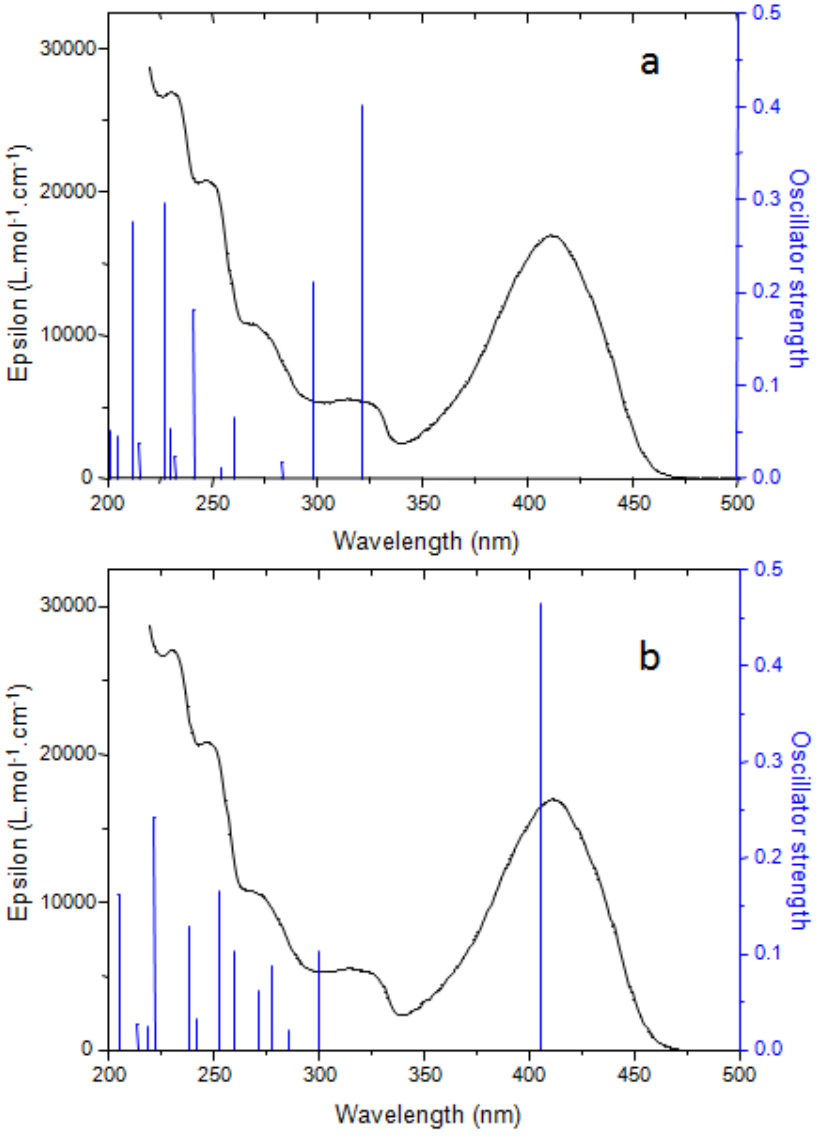
a
b
Epsilon (L.mol-1.cm-1)
Oscillator strength
Wavelength (nm)
0
10000
20000
30000
0.0
0.1
0.2
0.3
0.4
0.5
200
250
300
350
400
450
500

Fig. 3

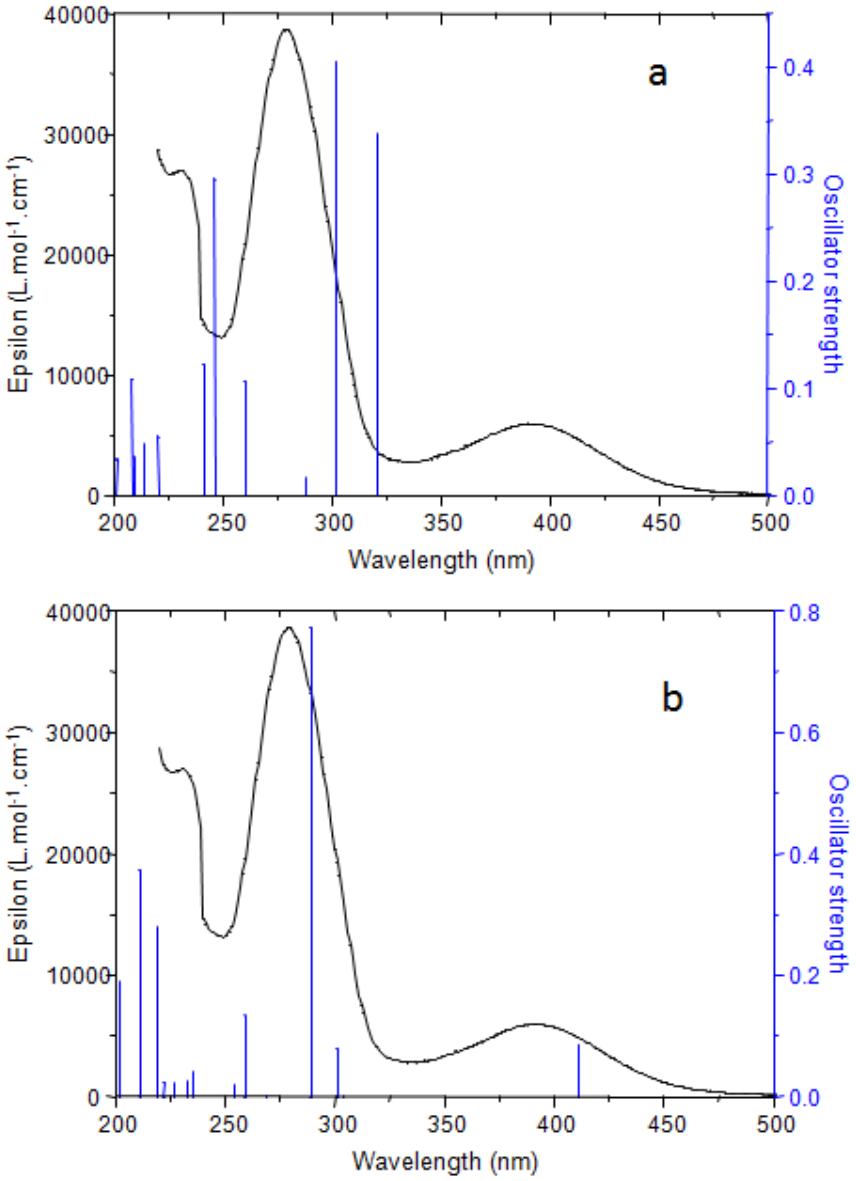
a
Epsilon (L.mol-1.cm-1)
Oscillator strength
Wavelength (nm)
b
Epsilon (L.mol-1.cm-1)
Oscillator strength
Wavelength (nm)

Fig. 4

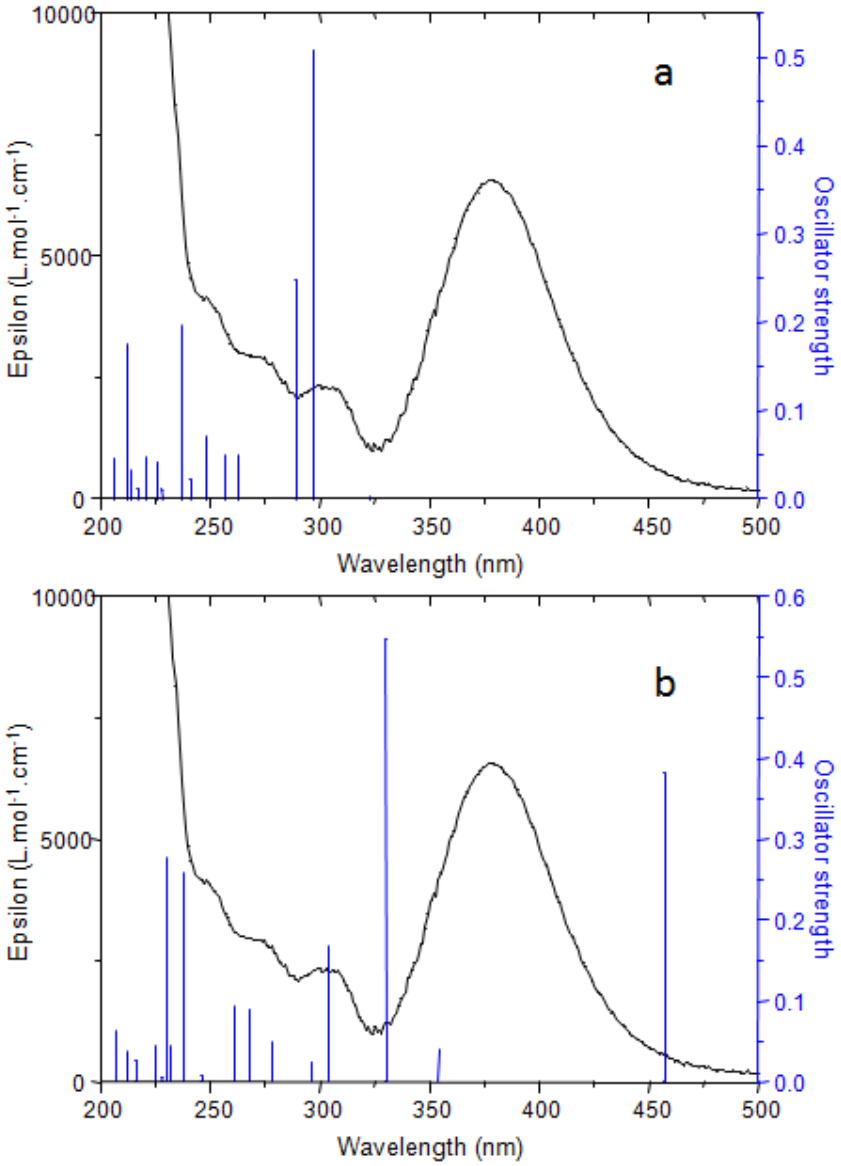
a
Epsilon (L.mol-1.cm-1)
Oscillator strength
Wavelength (nm)
b
Epsilon (L.mol-1.cm-1)
Oscillator strength
Wavelength (nm)

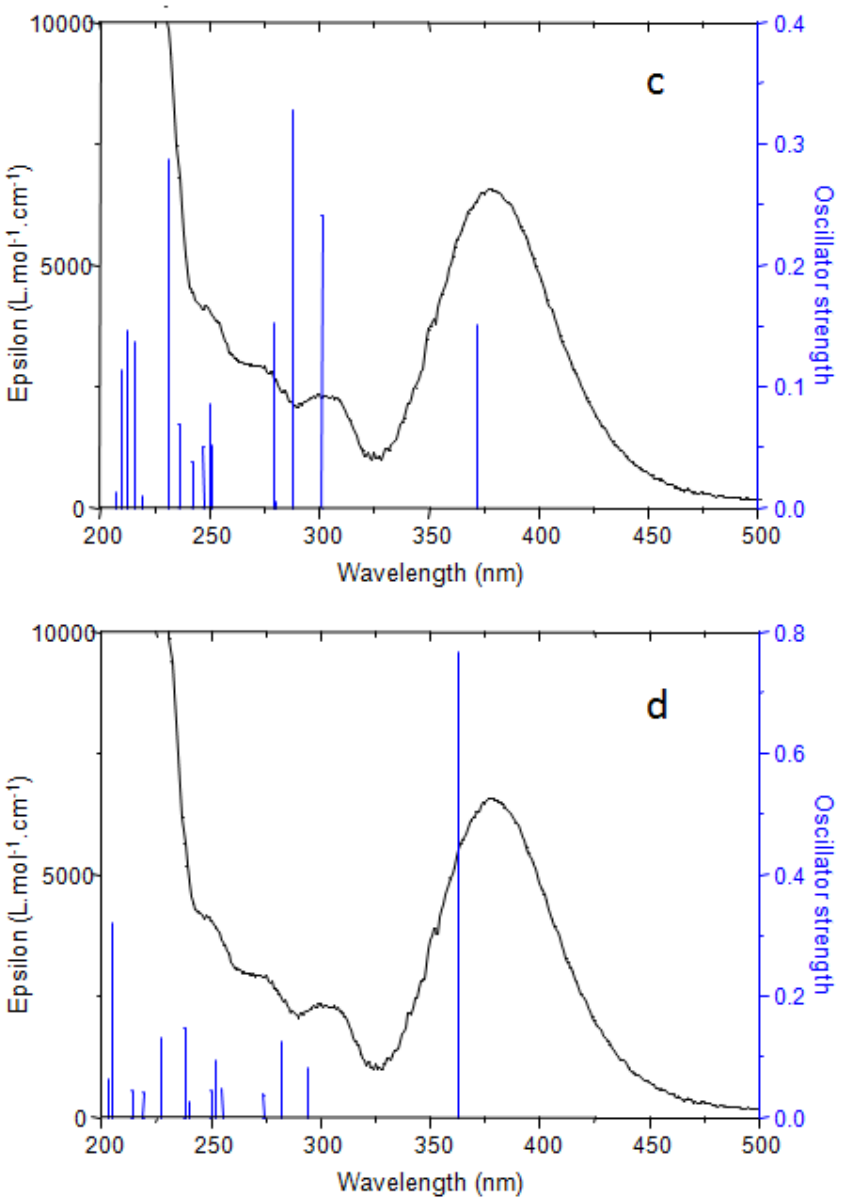
c
Epsilon (L.mol-1.cm-1)
Oscillator strength
Wavelength (nm)
d
Epsilon (L.mol-1.cm-1)
Oscillator strength
Wavelength (nm)

Fig. 5

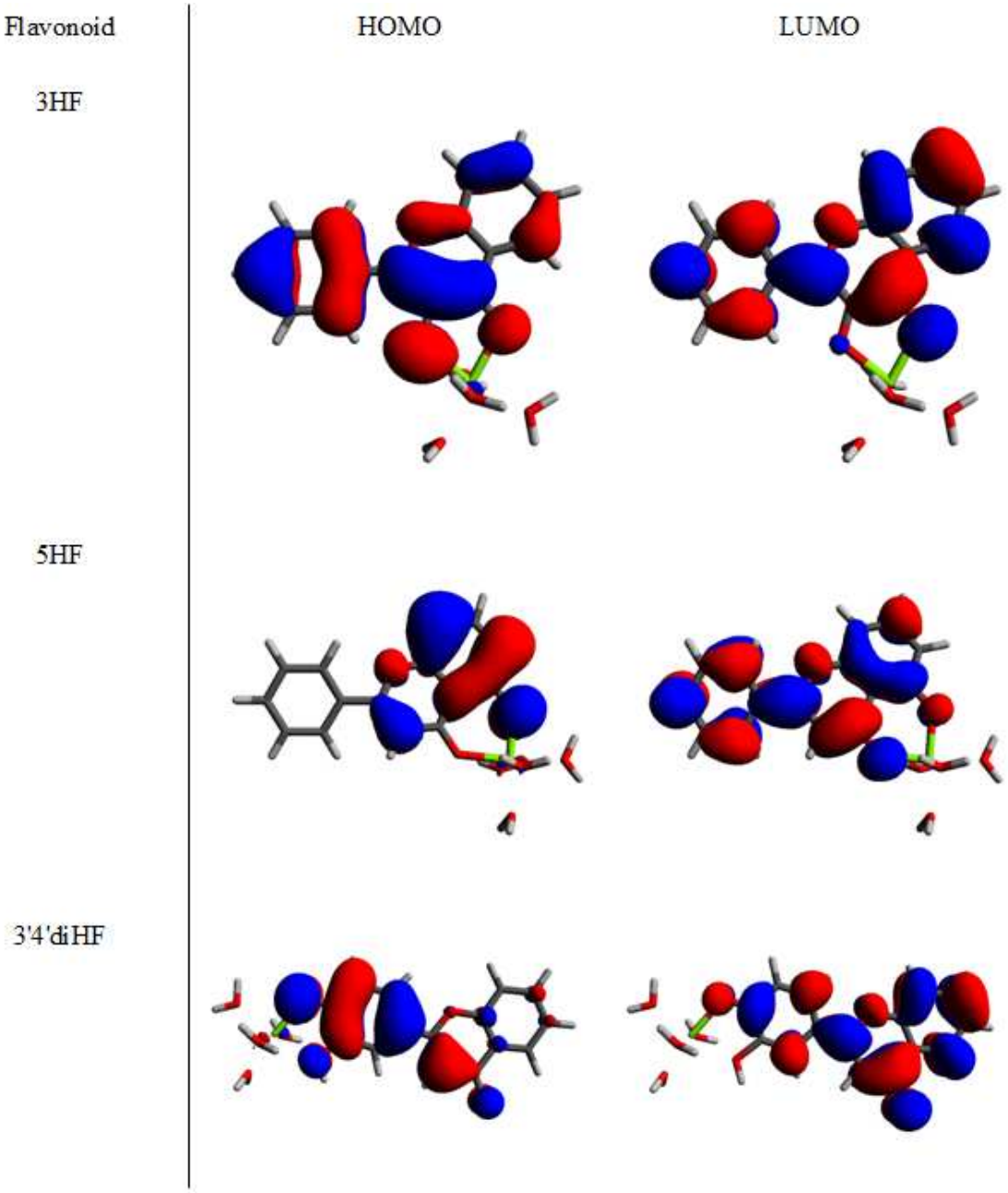

Fig. 6

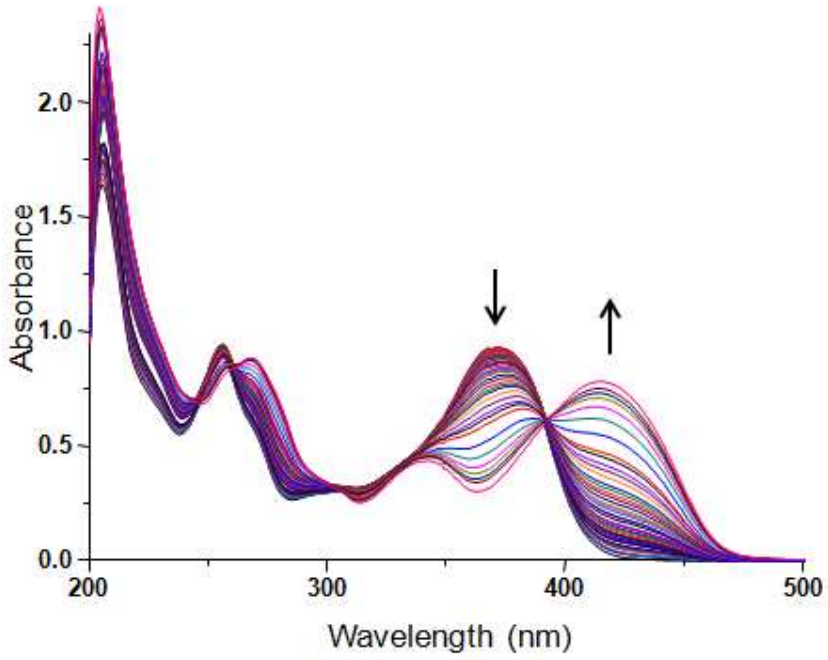

Fig. 7

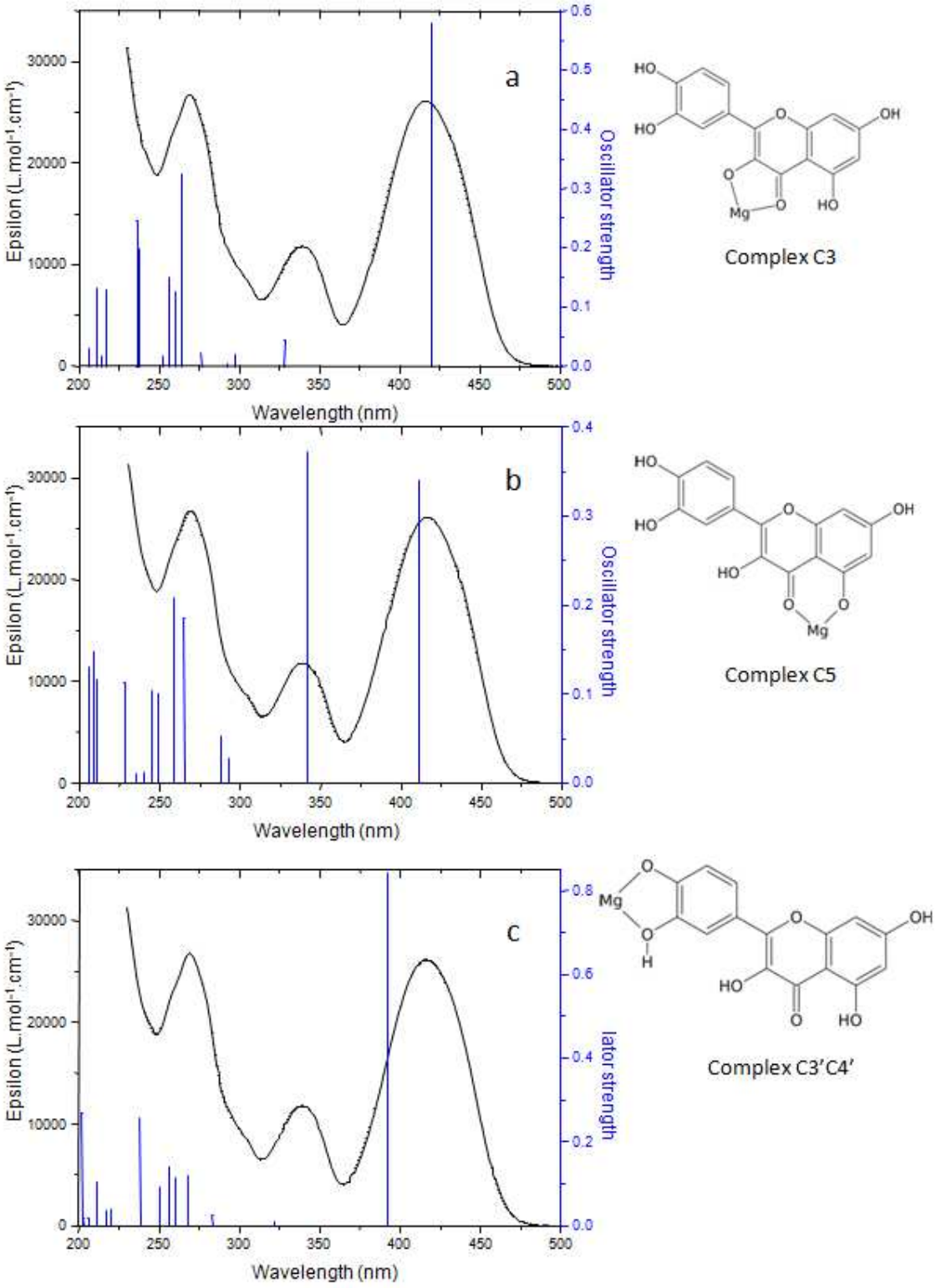
a
Epsilon (L.mol-1.cm-1)
Oscillator strength
Wavelength (nm)
Complex C3
b
Epsilon (L.mol-1.cm-1)
Oscillator strength
Wavelength (nm)
Complex C5
c
Epsilon (L.mol-1.cm-1)
lator strength
Wavelength (nm)
Complex C3'C4'

Fig. 8

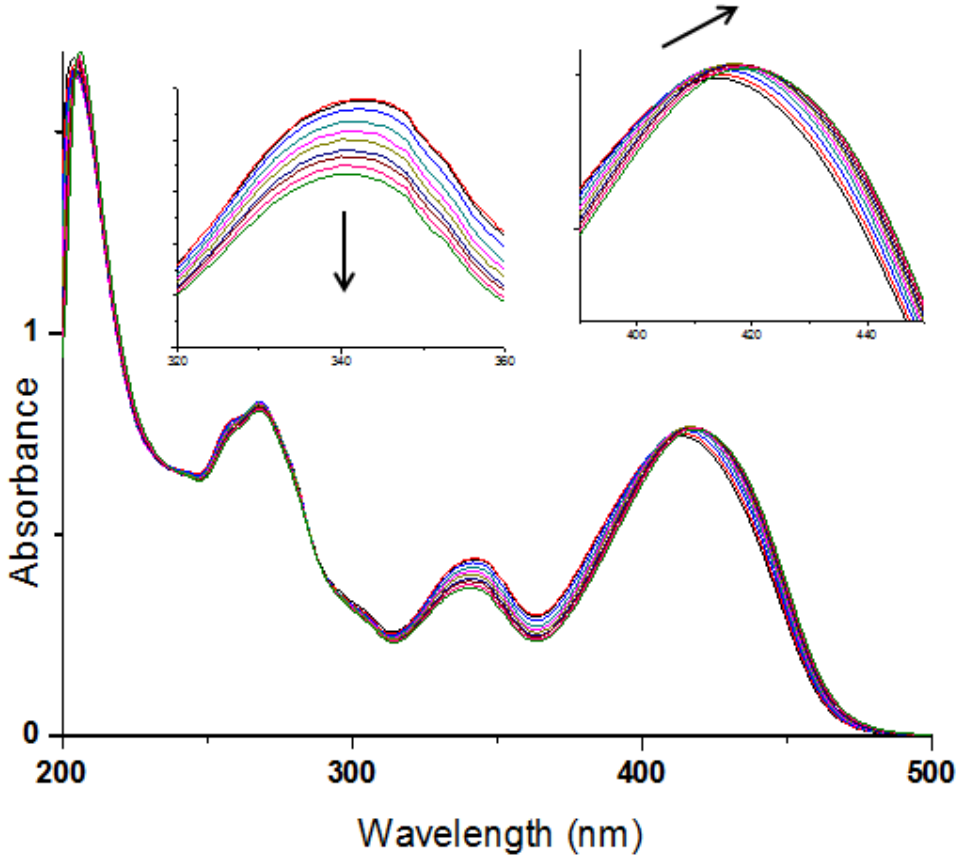
Absorbance
Wavelength (nm)
0
1
200
300
400
500
320
340
360
400
420
440

Fig. 9

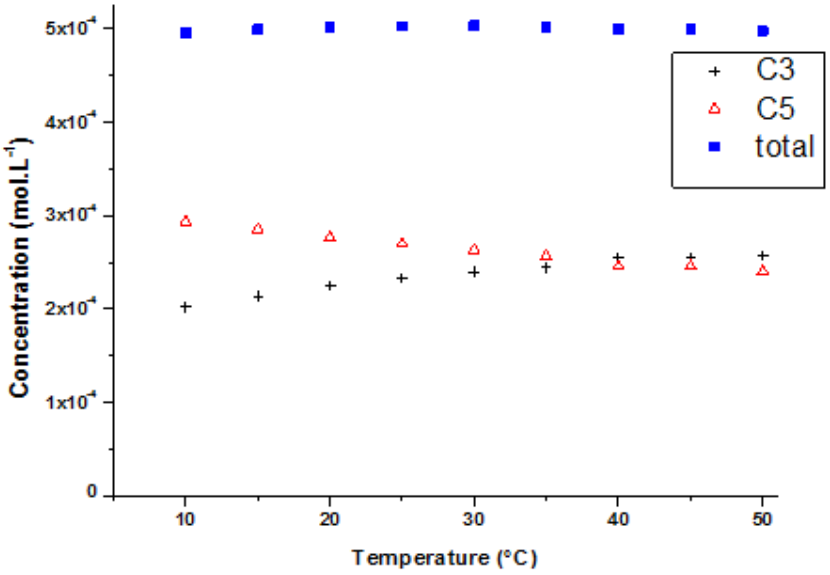
5x10⁻⁴
4x10⁻⁴
3x10⁻⁴
2x10⁻⁴
1x10⁻⁴
0
Concentration (mol.L⁻¹)
10
20
30
40
50
Temperature (°C)
C3
C5
total

Fig. 10

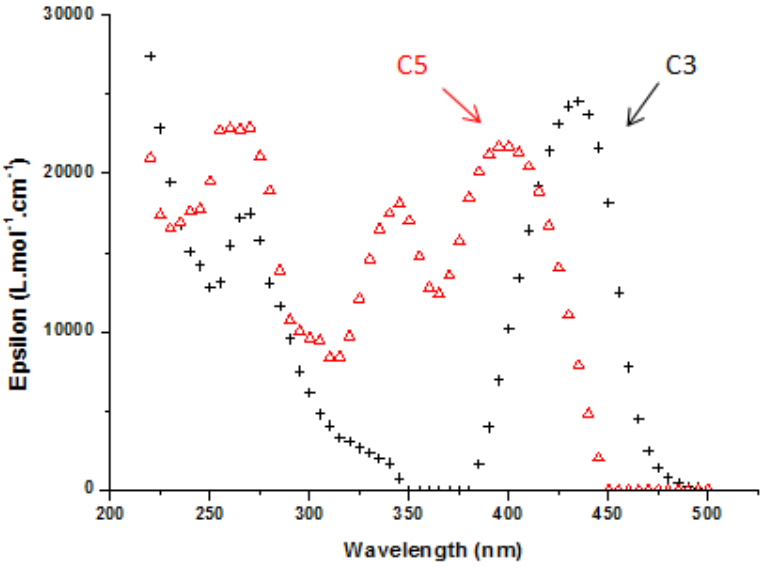
C5
C3
Epsilon (L.mol-1.cm-1)
Wavelength (nm)
30000
20000
10000
0
200
250
300
350
400
450
500

Fig. 11

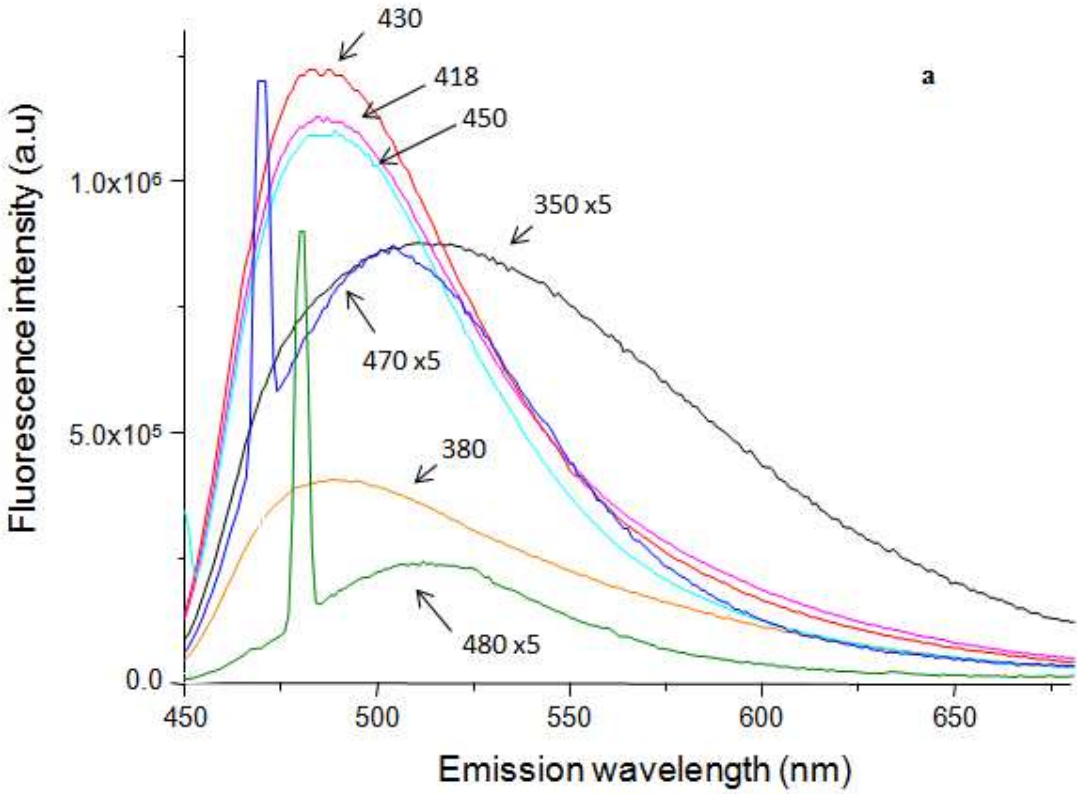
430
418
450
350 x5
470 x5
380
480 x5
a
Fluorescence intensity (a.u)
1.0x10⁶
5.0x10⁵
0.0
450
500
550
600
650
Emission wavelength (nm)

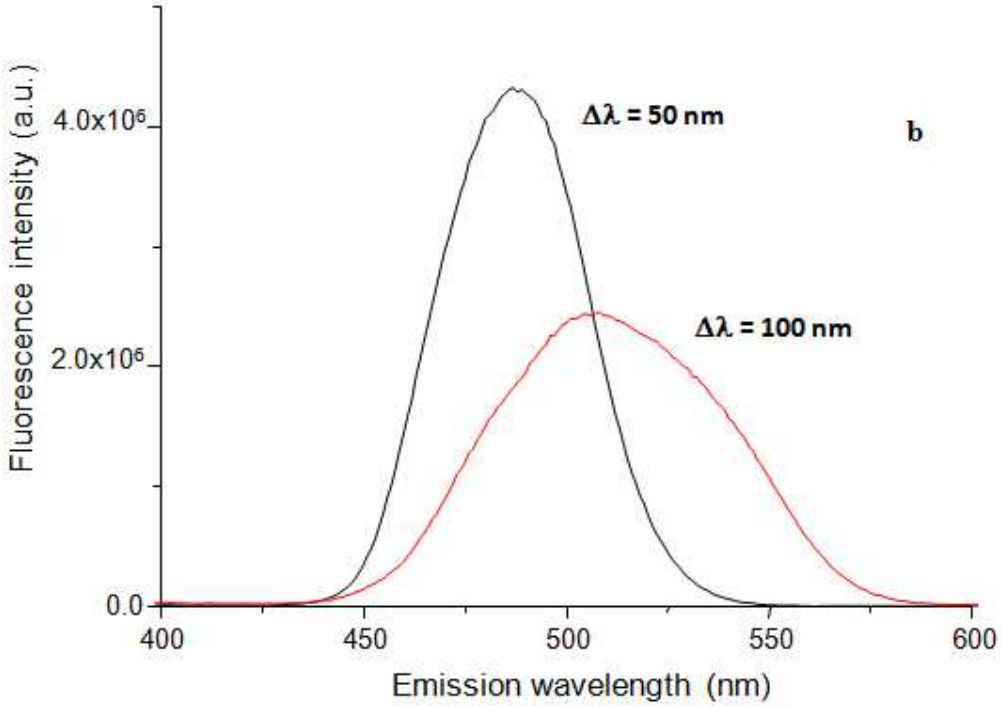
Δλ = 50 nm
Δλ = 100 nm
b
Fluorescence intensity (a.u.)
4.0x10⁶
2.0x10⁶
0.0
400
450
500
550
600
Emission wavelength (nm)

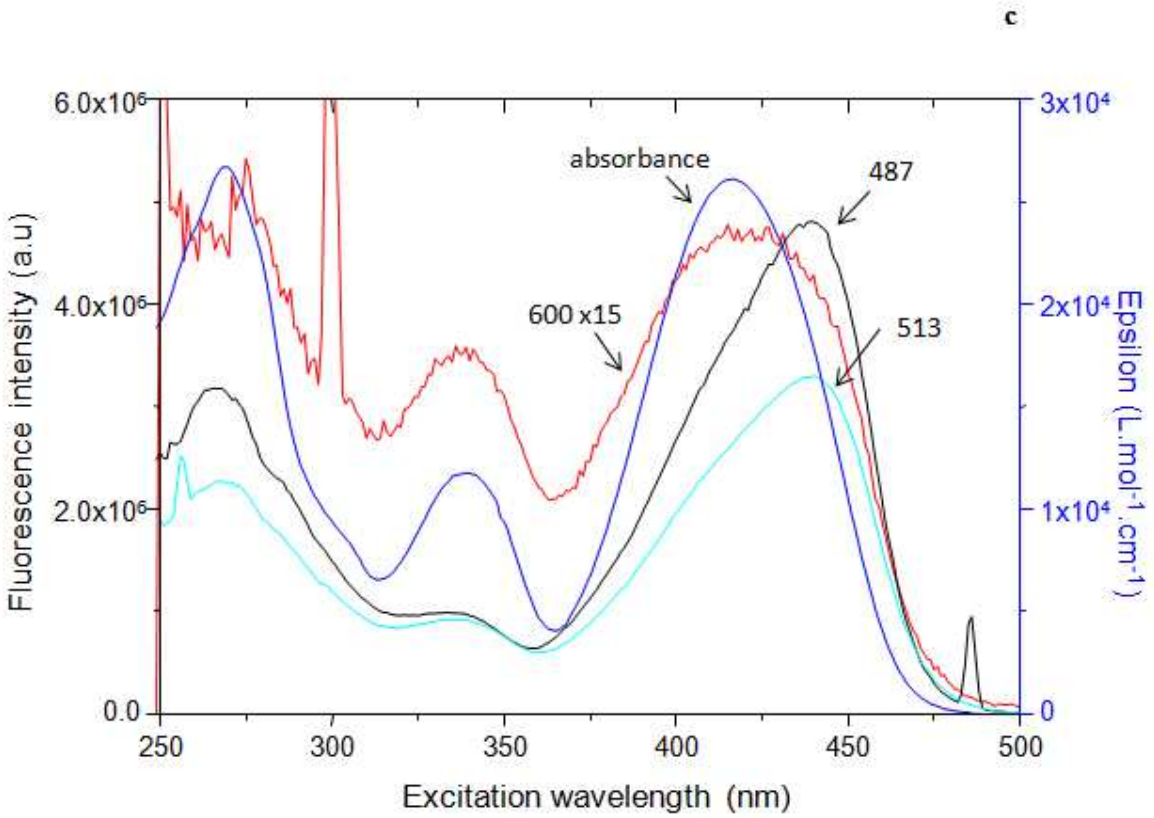
c
6.0x10⁶
4.0x10⁶
2.0x10⁶
0.0
Fluorescence intensity (a.u)
3x10⁴
2x10⁴
1x10⁴
0
Epsilon (L.mol⁻¹.cm⁻¹)
absorbance
487
600 x15
513
250
300
350
400
450
500
Excitation wavelength (nm)

Fig. 12